

G4-Quartet·M⁺ Borate Hydrogels

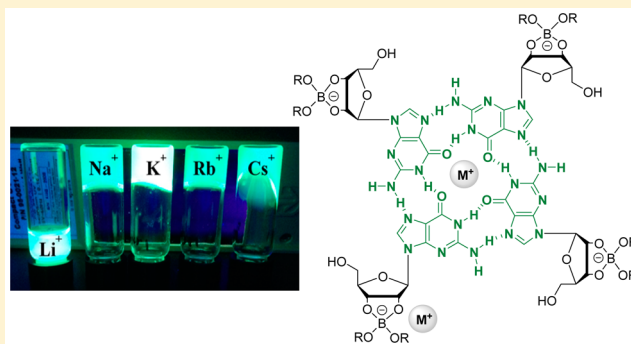
Gretchen Marie Peters,[†] Luke P. Skala,[†] Taylor N. Plank,[†] Hyuntaek Oh,[‡] G. N. Manjunatha Reddy,[§] Andrew Marsh,[#] Steven P. Brown,[§] Srinivasa R. Raghavan,[‡] and Jeffery T. Davis^{*†}

[†]Department of Chemistry & Biochemistry and [‡]Department of Chemical & Biomolecular Engineering, University of Maryland, College Park, Maryland 20742, United States

[§]Department of Physics and [#]Department of Chemistry, University of Warwick, Coventry CV4 7AL, U.K.

Supporting Information

ABSTRACT: The ability to modulate the physical properties of a supramolecular hydrogel may be beneficial for biomaterial and biomedical applications. We find that guanosine (G 1), when combined with 0.5 equiv of potassium borate, forms a strong, self-supporting hydrogel with elastic moduli >10 kPa. The counteraction in the borate salt (MB(OH)₄) significantly alters the physical properties of the hydrogel. The gelator combination of G 1 and KB(OH)₄ formed the strongest hydrogel, while the weakest system was obtained with LiB(OH)₄, as judged by ¹H NMR and rheology. Data from powder XRD, ¹H double-quantum solid-state magic-angle spinning (MAS) NMR and small-angle neutron scattering (SANS) were consistent with a structural model that involves formation of borate dimers and G4·K⁺ quartets by G 1 and KB(OH)₄. Stacking of these G4·M⁺ quartets into G4-nanowires gives a hydrogel. We found that the M⁺ cation helps stabilize the anionic guanosine-borate (GB) diesters, as well as the G4-quartets. Supplementing the standard gelator mixture of G 1 and 0.5 equiv of KB(OH)₄ with additional KCl or KNO₃ increased the strength of the hydrogel. We found that thioflavin T fluoresces in the presence of G4·M⁺ precursor structures. This fluorescence response for thioflavin T was the greatest for the K⁺ GB system, presumably due to the enhanced interaction of the dye with the more stable G4·K⁺ quartets. The fluorescence of thioflavin T increased as a function of gelator concentration with an increase that correlated with the system's gel point, as measured by solution viscosity



INTRODUCTION

Understanding molecular recognition and self-assembly processes is key for building functional materials such as supramolecular hydrogels.¹ Supramolecular hydrogels are colloidal networks composed of molecular building blocks that self-assemble into a fiber network that can entrap relatively large amounts of water.² Entanglement of these fibers leads to a hydrogel, one that is typically 98% water by weight, but is self-supporting and does not flow freely. Because the supramolecular assemblies that define the gel's network are held together by noncovalent interactions, supramolecular gelation is a dynamic and reversible process that may respond to stimuli, such as pH, light, enzyme activity, ions or temperature.^{3–8} Responsive and dynamic hydrogels are understandably attractive for many applications, including sensing of biomolecules and ions, as media for cell culture, tissue engineering and targeted drug delivery.^{1,9–14}

Supramolecular hydrogels made from biomolecules are of particular interest for in vivo applications.^{15,16} Water-soluble derivatives of guanosine, such as 5'-guanosine monophosphate (5'-GMP) have been known to form gels for over a century.¹⁷ Gelation of water and organic solvents by guanine derivatives has led to a number of interesting systems.^{11,18–37} Gelation by

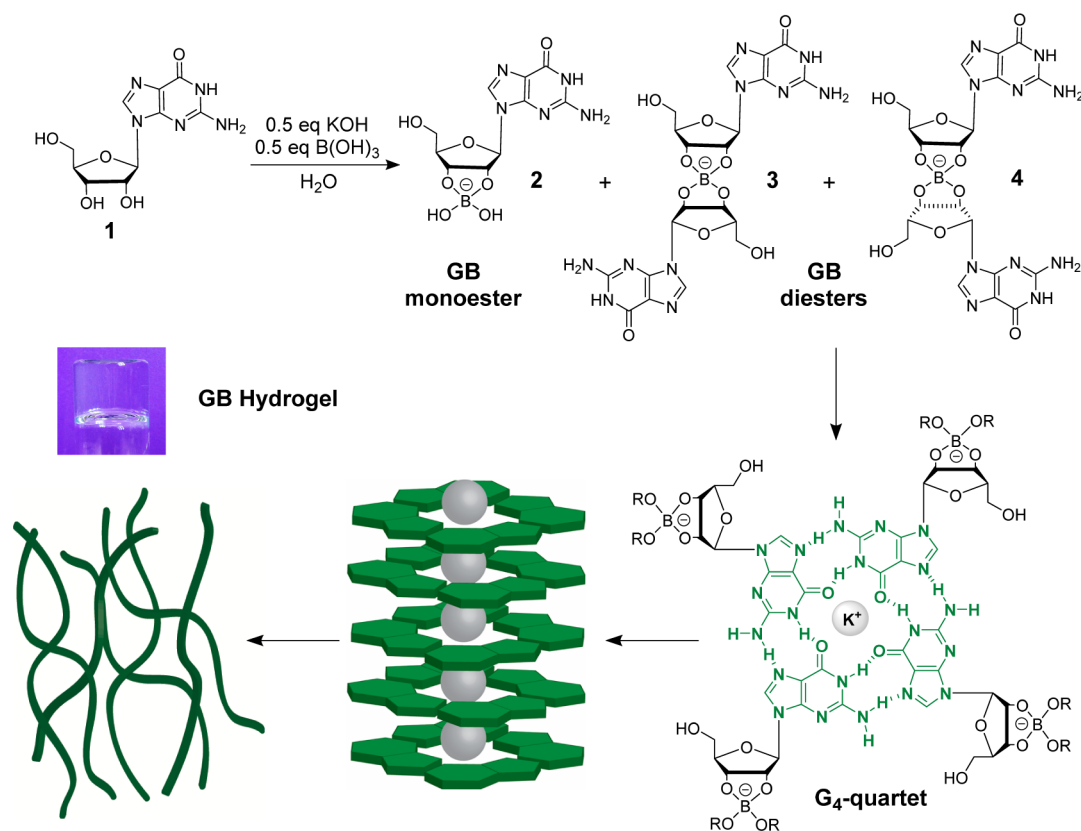
guanine analogues typically involves templating of G4-quartet motifs by cations such as K⁺ and Na⁺, where four guanine bases form a noncovalent macrocycle that is held together by hydrogen bonds and ion-ligand dipole interactions. The cations further assist the stacking of individual G4-quartets to give extended G4-wires, which ultimately form the fibers that underlie hydrogel formation. However, to gel water with 5'-GMP and other guanosine analogues one typically needs to use relatively high concentrations of the nucleobases gelator (generally >0.05 M) and KCl (0.1–0.5 M). This requirement is likely because of the stiff competition from water that makes formation of the G4-quartet's hydrogen bonds and ion-dipole interactions challenging. If one could enhance these noncovalent interactions in such a polar environment, hydrogelation would be easier. Dimerization of the guanosine gelators, using dynamic covalent bonds is one way to favor hydrogel formation at lower gelator concentrations.^{8,38}

We recently reported studies on a G4·K⁺ hydrogel, one in which gelation of water by guanosine (G 1) itself is achieved by addition of just 0.5 equiv of KB(OH)₄ relative to the

Received: March 16, 2015

Published: April 14, 2015

Scheme 1. Proposed Mechanism for Gelation of Water by G 1 and $\text{KB}(\text{OH})_4$, via Formation of GB Borate Diesters 3/4, Followed by Formation and Stacking of $\text{G4}\cdot\text{M}^+$ Quartets and Intermolecular Association of G4 -Wires



concentration of the gelator G 1.^{25,26,39} As shown in Scheme 1, we proposed that hydrogelation is due to the borate anion's ability to promote dimerization of G 1 in water, which then facilitates the subsequent self-assembly of G 1 that leads to hydrogel formation. Borate esters are anionic, tetravalent species formed by reaction of *cis*-1,2-diols with $\text{B}(\text{OH})_3$ or $\text{B}(\text{OH})_4^-$. Borate-diol chemistry has been applied extensively to numerous processes in water, including chromatographic separation of sugars and nucleosides,⁴⁰ modulation of sugar conformation to direct reaction progression,^{41,42} and templation of base-pairs by nucleic acid analogues.⁴³ As depicted in Scheme 1, borate esters formed from reaction of G 1 and $\text{B}(\text{OH})_4^-$ can exist as either monomers or dimers. Depending on the solution conditions, a GB monoester 2, formed by initial reaction of $\text{B}(\text{OH})_4^-$ with G 1, is able to chelate a second guanosine, giving rise to diastereomeric GB diesters 3 and 4. We proposed that the GB diesters 3/4 are crucial to formation of the supramolecular network that gels water. In this system, formation of the anionic GB diesters 3/4 helps dissolve G 1, a notoriously insoluble compound, in water. We also hypothesized that GB diesters 3 and 4 are the building blocks that ultimately result in the formation of GB hydrogels, a system with enhanced stability and unique physical properties when compared to other G₄ gels. For example, these GB hydrogels are indefinitely stable when suspended in 155 mM KCl solution. Because the GB-K⁺ hydrogel is anionic and remains intact in salt water it is able to selectively extract cationic compounds from solution and incorporate those compounds into its network. Moreover, *cis*-1,2-diols other than G 1 can be incorporated into the GB hydrogels, presumably by forming covalent linkages with some of the tetravalent borates that are

in the gel network. These unique properties may make the GB hydrogels attractive for sensing and drug delivery applications.

In our initial report we proposed the mechanism for formation of GB hydrogels from G 1 and $\text{KB}(\text{OH})_4$ that is shown in Scheme 1. Now, in this paper, we describe efforts to test whether Scheme 1 is a reasonable mechanism. Experiments in this paper have led to further insight into how individual components, such as the borate salt $\text{M}^+ \text{B}(\text{OH})_4^-$, and proposed intermediates, such as the GB diesters 3/4, the $\text{G4}\cdot\text{M}^+$ quartets and the stacks of G₄ quartets, help define the structure and properties of these GB hydrogels. For example, we have expanded characterization of the hydrogel by using solid-state NMR and powder X-ray diffraction to obtain molecular-level evidence for G₄-quartet formation and stacking of G₄-quartet units. We have also used small angle neutron scattering (SANS) to get information about the dimensions of the hydrogel fibers, data that is consistent with our structural model. Such studies have revealed that changing a single component can result in significant changes in macroscopic properties. For example, G 1 and $\text{KB}(\text{OH})_4$, when mixed in water at the right concentration and stoichiometry, give a remarkably sturdy hydrogel. But, replacing $\text{KB}(\text{OH})_4$ with $\text{LiB}(\text{OH})_4$ gives a material that is more like a viscous liquid rather than a gel. Finally, we have continued our exploration of studying how cationic dyes interact with the anionic GB hydrogel. We have found that thioflavin T (ThT) shows a large increase in fluorescence in the presence of G 1 and borate salts, presumably by binding G₄-quartet assemblies. This ThT response is sensitive to the cation used in the hydrogel recipe, and we have found that ThT can be used to monitor the hydrogelation process that is promoted by G 1 and borate salts.

RESULTS AND DISCUSSION

Solid-State ^1H NMR Confirms the Presence of Stacked G4-Quartets in the GB Hydrogel. Key to the hierarchical hydrogel formation by G 1 and $\text{KB}(\text{OH})_4$ is the assembly of stacked G4-quartets that provide the core of the hydrogel's fibers. In our initial communication we provided CD evidence for G4-quartet stacking.²⁶ Now, we show powder X-ray diffraction (PXRD) and solid-state NMR data that is consistent with the stacking of G4-quartets in the GB hydrogel. PXRD data obtained from a freeze-dried sample of a GB hydrogel formed from G 1 and 0.5 equiv of $\text{KB}(\text{OH})_4$ showed a significant peak at $2\theta \approx 26.8^\circ$ ($d = 3.3 \text{ \AA}$), which is in line with the π - π stacking distance between two planar G4-quartets (Figure S1, Supporting Information).

In addition to PXRD analysis, magic-angle spinning (MAS) ^1H NMR also provided evidence for the formation and stacking of G4-quartets.⁴⁴ ^1H double-quantum (DQ) MAS spectroscopy is a powerful probe of proton-proton proximities in the solid state,⁴⁵ and the technique has been recently used to distinguish G4-quartet from G-ribbon structures in supramolecular assemblies formed by lipophilic guanosine analogues.⁴⁶ Figure 1 presents a ^1H DQ-SQ (single-quantum) correlation spectrum

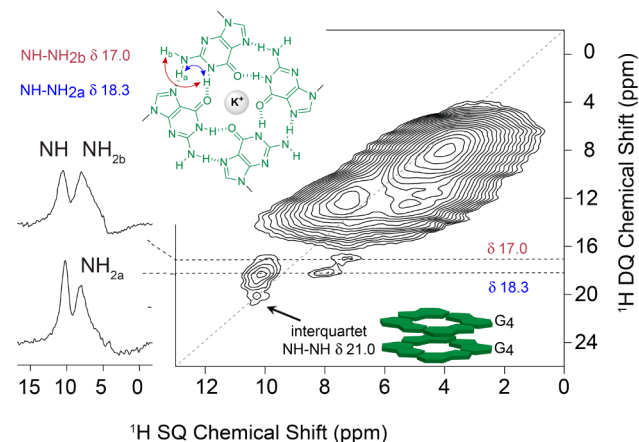


Figure 1. ^1H (600 MHz) 2D DQ-SQ MAS (60 kHz) NMR correlation spectrum of a lyophilized powder from a 2 wt % G 1- $\text{KB}(\text{OH})_4$ hydrogel. Extracted rows at the stated DQ frequencies (in ppm) are shown. The $F_1 = 2F_2$ diagonal is drawn as a dashed line, and base contour level is at 1.1% of maximum peak height.

for a lyophilized 2 wt % G 1- $\text{KB}(\text{OH})_4$ hydrogel, recorded at a ^1H Larmor frequency of 600 MHz and MAS frequency of 60 kHz. In DQ-SQ MAS spectra, peaks are observed in the DQ dimension as the sum of the SQ chemical shifts for pairs of hydrogens in proximity ($<3.5 \text{ \AA}$).⁴³

Consider the region of the spectrum in Figure 1 that corresponds to the imino NH1 (10.5 ppm) and amino $\text{NH}_{2a,b}$ and aromatic protons H8 (6–9 ppm). Rows that arise from DQ-SQ correlation peaks are plotted on the left. The DQ peaks at $\delta_{\text{DQ}} 17.0$ ppm and $\delta_{\text{DQ}} 18.3$ ppm correspond to intramolecular NH1–NH2 interactions, with DQ chemical shifts that are diagnostic of the G4-quartet's hydrogen-bonded structure.⁴⁵ This DQ-SQ spectrum also shows another important feature, namely, a DQ peak at $\delta_{\text{DQ}} 21.0$ ppm, which we interpret as corresponding to an intermolecular NH1–NH1 interaction between stacked G4-quartets ($\delta_{\text{DQ}} = 10.5 + 10.5 = 21$ ppm). In summary, this ^1H NMR data (1) establishes that the GB hydrogel contains stacked G4-quartets

and (2) expands the use of ^1H MAS DQ-SQ to identify structural elements in supramolecular hydrogels.

Small-Angle Neutron Scattering Data Is Consistent with a G4-Based Hydrogel. With evidence for G4-quartets in the solid state, we next examined the morphology of the elements in the gel. In supramolecular gels, the gelator molecules self-assemble into fibers, which then together form a three-dimensional network that is referred to as a self-assembled fibrillar network (SAFiN). For the GB hydrogel, this SAFiN likely arises from G4-quartets that stack to give G4-wires, which can then form fibrils that entangle into a network (Scheme 1). We previously obtained images of this fibril network by using cryoTEM.²⁶ The hydrogel's entangled fibers were 4–6 nm in width and were μm in length. In this paper, we now describe more data about the SAFiN by comparing small angle neutron scattering (SANS) data of the GB hydrogel with SANS data obtained from another well-characterized G4 hydrogel, one formed from a binary mixture of triacetylguanosine (TAcG 5) and guanosine (G 1).^{22,23}

The SANS data on both these gels is shown in Figure S2 (Supporting Information). These data were fit to a model for discrete semiflexible chains. From the model fits, radii (r) and persistence lengths (L) of the chains were obtained and are shown in Table 1 for the K^+ GB hydrogel (2 wt % G 1) and the

Table 1. SANS-Derived Radii and Persistence Lengths of Fibrils from Hydrogels (a) G 1- $\text{KB}(\text{OH})_4$ and (b) a 1:1 Binary Mixture of TAcG 5 and G 1 with KCl

Gel	r (Å)	L (Å)
GB (K^+)	21.5	460
TAcG 5:G 1	16.9 (14.7) ^a	355 (320) ^a

^aValues in parentheses were reported in ref 22.

binary TAcG 5:G 1 hydrogel (1:1 mix; 2 wt %). The fibers in the GB hydrogel were found to have a radius of 21.5 Å and a persistence length of 460 Å. These values are consistent with fiber dimensions from our previous cryoTEM analysis of the GB hydrogel.²⁶ The TAcG 5:G 1 binary gel, which serves as a control here, had chains with a significantly smaller radius (16.9 Å).²²

Adopting the core-shell model developed by Rowan for the structure of the TAcG 5:G 1 binary hydrogel,²² we used our SANS data to provide insight into structural differences between the GB hydrogel and the control gel (TAcG 5:G 1). In this core-shell model, the nucleobases of the G4-quartet are proposed to form the core of the hydrogel's fiber and the attached sugars make up the shell. For the TAcG 5:G 1 binary gel, Rowan previously proposed that the radii of both the G4-quartet core and the surrounding ribose shell was between 7 and 8 Å.²²

From the SANS data that we collected on the 2 samples (Table 1), the radius of the GB fibers is about ~1.3 times that of the TAcG 5:G 1 fibers. Since the G4-quartet cores of both hydrogels are identical, the SANS data indicates that, relative to the TAcG 5:G 1 control sample, the GB fibers must have an expanded ribose shell. This expanded shell for the GB fibers, as illustrated in Figure 2, is consistent with a second ribose being covalently attached because of the borate diester linkage. Thus,

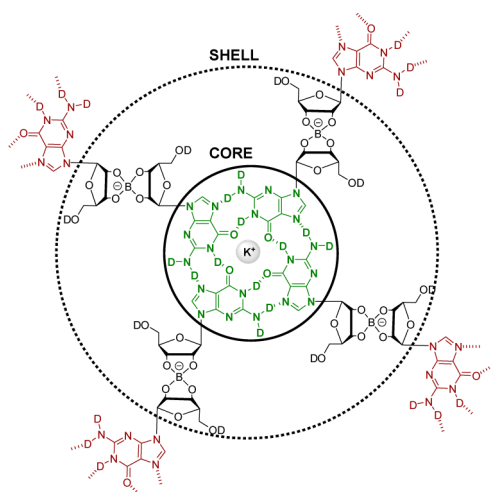


Figure 2. Illustration of the core–shell model as applied to the GB (K^+) hydrogel. This model is consistent with fiber dimensions determined from SANS data on hydrogel samples made from (a) G 1· $KB(OH)_4$ and (b) a 1:1 binary mixture of TAcG 5 and G 1. Labile hydrogens are replaced by deuterium, as the samples were prepared in D_2O .

overall, the SANS data is consistent with the structural model we propose in Scheme 1 and Figure 2.

Rheology Shows That G 1· $KB(OH)_4$ Is a Strong Hydrogel. Having established the presence of a fibrous network composed of G_4 -quartets, we next sought to examine these hydrogels on the macroscopic scale. The fibrous network of a hydrogel typically results in the material exhibiting solid-like rheology.^{1,2} That is, when examined as a function of frequency, the storage modulus (G') of the material should remain larger than its loss modulus (G''), and moreover, G' should be independent of frequency, indicating that the fibrous network does not relax even over long time scales. With this in mind, we examined the rheological properties of the G 1· $KB(OH)_4$ hydrogel and compared it to the material made from G 1 and $LiB(OH)_4$, which by manipulation and visual observation we knew to be weaker than the G 1· $KB(OH)_4$ hydrogel. Both were studied at a concentration of 2 wt %.

As shown in Figure 3A, dynamic frequency sweeps indicate that the K^+ GB hydrogel has an elastic response that is essentially independent of frequency over the entire range of frequencies tested. Furthermore, the 2 wt % K^+ hydrogel has a storage modulus (G') of ~ 11 kPa, suggesting that it is a strong hydrogel. This is consistent with the fact that the material holds its weight in an inverted vial for extended periods of time. Oscillatory stress sweeps reiterate this finding in that the yield stress of the K^+ material, i.e., the stress at which G' rapidly plummets, is ~ 400 Pa (Figure 3B). In contrast, the Li^+ GB system has a G' that is much closer to G'' and both moduli vary substantially with frequency. Oscillatory stress sweeps on the Li^+ GB show a gradual decrease in G' with stress rather than the yielding behavior seen with the K^+ GB material. These rheological data not only demonstrate that the K^+ GB system is a robust hydrogel, but also emphasizes the cation's importance in defining the structure and properties of these $G_4\cdot M^+$ borate hydrogels.

1H Solution-State NMR Shows That the Cation Is Important in Stabilizing $G_4\cdot M^+$ Borate Hydrogels. Rheology clearly showed that the macroscopic properties of materials made from G 1 are different depending on whether $KB(OH)_4$

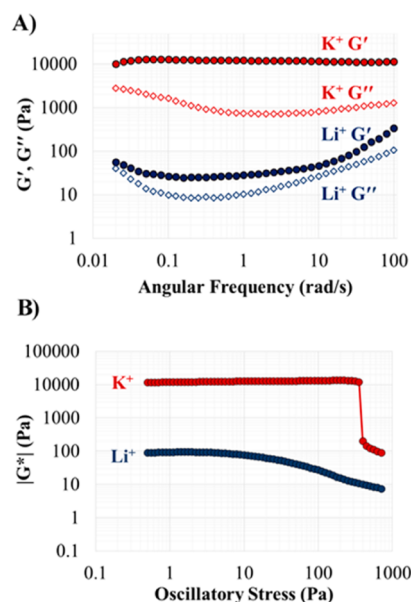


Figure 3. Dynamic frequency sweeps (A) and oscillatory stress sweeps (B) of 2 wt % K^+ and Li^+ GB hydrogels (72 mM G 1, 36 mM $MB(OH)_4$).

or $LiB(OH)_4$ is added. We next sought to determine the role of the alkali metal cation in stabilizing these $G_4\cdot M^+$ borate hydrogels at the molecular-level. To start, we visually assessed gelation of a 2 wt % solution of G 1 that contained different alkali borate salts. As shown in Figure 4A, after allowing the samples to sit at room temperature for 4 h, the Na^+ , K^+ , Rb^+

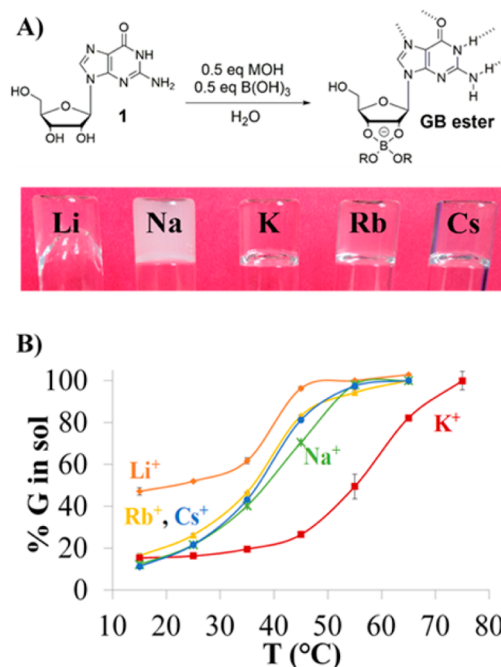


Figure 4. Cation's identity alters the physical properties of a GB hydrogel. (A) Inverted vials of 2 wt % GB $MB(OH)_4$ gels [$M = Li, Na, K, Rb, Cs$] after 4 h at rt. (B) Melting curves for GB gels formed with G 1 (50 mM) and $MB(OH)_4$ [$M = Cs, Rb, K, Na, Li$] (25 mM), as determined by 1H NMR. While the K^+ gel melts around ~ 57 °C, the T_m of the other M^+ gels is ~ 15 – 20 °C lower ($Li \approx 37$ °C, Rb and $Cs \approx 38$ °C, and $Na \approx 41$ °C \pm 10%).

and Cs⁺ systems all formed hydrogels of varying opacity (vials Na, K, Rb, and Cs, respectively). Specifically, while the K⁺ hydrogel is entirely transparent, GB gels formed with NaB(OH)₄ are turbid and cloudy. Additionally, the Li⁺ system can be seen to be flowing down the side of the vial in Figure 4A, indicating its viscoelastic character. The Li⁺ system does eventually form a nonflowing and transparent GB hydrogel, given longer times to stand, but its structure is very weak. That is, upon agitation, the Li⁺ GB hydrogel rapidly forms a nonviscous, free-flowing solution, and does not revert to a gel thereafter. We are currently in the process of further characterizing and exploiting this unique behavior.

While visual observations from “inverted vial” tests suggested that the K⁺ GB hydrogel was stronger than those formed with other alkali cations, we sought to quantify the cation’s influence by comparing the gel–sol transition temperatures (T_m) obtained from variable temperature solution-state ¹H NMR (VT-NMR) experiments (Figure 4B). In these VT-NMR experiments, we measured the amount of G 1 in the sol as a function of temperature by integrating the NMR signals for G 1 and its borate esters 2–4. As the temperature increased, the gel phase melted and transformed into a sol.^{8,19} As the temperature approaches the gel–sol transition temperature (T_m), the % of total G 1 in the sol phase dramatically increases. This transition temperature is the point at which half of the material initially in the gel has been released into the sol. Thus, comparing the observed T_m values from these VT-NMR melt curves allowed us to assess the relative stability of the different GB-M⁺ hydrogels.

As one might anticipate for an assembly built from G4-quartets, Figure 4B shows that the K⁺ GB hydrogels have the highest gel–sol temperature, with a T_m value of ~57 °C. In contrast, hydrogels formed from G 1 in the presence of other alkali metal borates (Li⁺, Na⁺, Rb⁺, Cs⁺) melted at temperatures that were below (~15–20 °C) the T_m value of the K⁺ GB gel. The biggest difference in T_m values was between the Li⁺ and K⁺ GB hydrogels. This is further evidenced by comparing the variation in % G 1 in the sol phase for each system. At 25 °C, over 80% of total G 1 is in the gel phase for the K⁺ GB system. Conversely, only about 48% of the G 1 is in the Li⁺ hydrogel at 25 °C, presumably resulting in the differences in strength and stability for the 2 systems.

On account of these variations in physical properties, we hypothesized that different M⁺ GB hydrogels might display detectable differences in structure that could help test our gelation mechanism in Scheme 1. We had proposed that hydrogelation by G 1 was triggered by formation of borate diesters 3/4 and subsequent self-association of those dimers into G4-quartets. In the next sections, we focus on whether different M⁺ GB hydrogels show observable changes in molecular structure, as detected by NMR.

¹H and ¹¹B Solution-State NMR Confirm That Guanosine Borate Diesters Are Key Components of the G4-K⁺ Hydrogels. The borate diesters 3/4 have been proposed, by us and others,^{25,26} to be important for hydrogel formation in the presence of G 1 (Scheme 1). In our initial report on these GB hydrogels, we used solid-state ¹¹B NMR,²⁶ to identify and distinguish ¹¹B signals for GB diesters 3/4 that were in the gel and sol phases. Furthermore, we found that stronger gels had higher percentages of the GB diester 3/4 in the gel phase, rather than in solution. We took this as evidence that GB diesters are essential for gelation.

As shown below, the key role of the GB diesters 3/4 in the hydrogelation triggered by G 1 and borate salts was illuminated when comparing VT ¹H and ¹¹B solution-state NMR spectra for GB hydrogels. These VT-NMR experiments allowed us to monitor the species in solution and, thus, indirectly determine what the major species were in the gel phase. For our initial studies, we began with VT ¹¹B and ¹H NMR on a gel formed using G 1 (50 mM) and NaB(OH)₄ (25 mM) in D₂O. The Na⁺ hydrogel was chosen because, unlike the sturdier K⁺ GB gel, it gave well-resolved NMR signals for all the low-molecular species involved in gelation: G 1, monoborate ester 2 and diborate esters 3/4. As shown in Figure 5, at temperatures

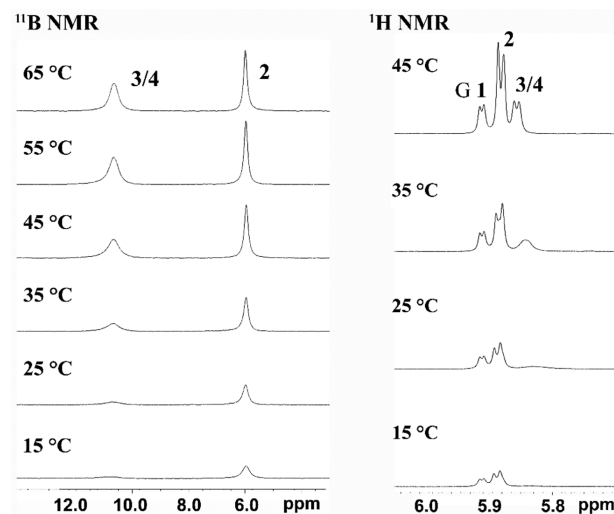


Figure 5. VT ¹¹B NMR spectra of G 1 (50 mM) and NaB(OH)₄ (25 mM) in D₂O recorded from 15 to 65 °C (left). At 15 °C, only the peak at δ 6.01 ppm is present, corresponding to monoester 2. At higher T (25–65 °C), an additional peak at δ 10.83 ppm appears for GB diesters 3/4. Similarly, VT ¹H NMR spectra at 15 °C show two doublets, one at δ 5.92 ppm, which correlates to free G 1 and the other at δ 5.89 ppm, which we assigned as the monoester 2. As the temperature is increased, a new peak appears (25–35 °C) and resolves into a doublet at δ 5.86 ppm by 45 °C. We assigned this peak as the GB diesters 3/4. Peaks were assigned on the basis of DOSY.

below 25 °C, we observed a single peak at δ 6.01 ppm (with BF₃·O(C₂H₅)₂ as reference). On the basis of our previous work with nucleoside-borate esters and literature precedent, we assigned this ¹¹B NMR signal to the GB monoester 2.^{26,47–49} As the temperature was increased, a second ¹¹B NMR peak at δ 10.83 ppm began to appear and increase in relative intensity. We assigned this signal at δ 10.83 ppm to the GB diesters 3/4, again based on literature precedent.

Additional structural information on the composition of the gel phase was obtained from VT ¹H NMR experiments, which we ran in parallel with the ¹¹B NMR VT studies. Again, as the gel melted, the ¹H NMR spectra changed significantly. We found the ribose H1' region to be ideal for monitoring these structural variations. At low temperatures ($T < 25$ °C), two discrete doublets are seen, one for monomeric borate ester 2 at δ 5.89 ppm ($d, J = 4.2$ Hz) and the other for “free” G 1 δ at 5.92 ppm ($d, J = 5.4$ Hz). As the sample was warmed, a new peak appeared; at 45 °C this new peak was a well-resolved doublet at δ 5.86 ppm ($d, J = 4.2$ Hz). We assigned this signal to the ¹H proton for borate diesters 3/4.

To corroborate assignments of the GB monoester **2** and diesters **3/4**, we measured diffusion coefficients at 45 °C for the resolved H1' peaks by diffusion-ordered NMR (DOSY). The largest diffusion coefficient ($6.050 \times 10^{-10} \text{ m}^2 \text{ s}^{-1}$), indicating that it is the smallest species in solution, corresponded to the peak at δ 5.92 ppm that we had assigned to G **1**. The diffusion coefficient for the peak at δ 5.89 ppm ($5.879 \times 10^{-10} \text{ m}^2 \text{ s}^{-1}$), which we had assigned to GB monoester **2**, was notably smaller than that of G **1**. The smallest diffusion constant ($4.823 \times 10^{-10} \text{ m}^2 \text{ s}^{-1}$) was for the peak at δ 5.86 ppm, signifying that it belongs to the largest species in solution, namely, the GB diesters **3/4**.

With our assignments confirmed by this diffusion NMR experiment, it became clear that the ^1H and ^{11}B VT-NMR data fully support our proposal that the GB borate diesters **3/4** drive the gelation mechanism. At temperatures that are well below the hydrogel's melting temperature, the sol phase is comprised of only GB monoester **2** and free G **1**. There is no borate diester **3/4** observed in solution at these lower temperatures, and thus the borate diesters must all be in the gel phase. However, as the temperature increases and the gel network starts to dissociate, the ^1H and ^{11}B NMR signals for GB diesters **3/4** appear and increase in intensity until the gel melts. This VT solution NMR data, combined with our previously reported solid-state MAS NMR data, indicates that GB diesters **3/4** are the primary guanosine and borate species within the GB hydrogel.

Additional KCl Strengthens the GB Hydrogels. Our data indicated that borate diesters **3/4** and the G4-quartet are important for hydrogel formation. But, we realized that there was not enough K^+ in a 2:1 mixture of G **1** and $\text{KB}(\text{OH})_4$ to fully stabilize all the anionic diesters **3/4** and fill all the G4-quartet units that would make up the hydrogel. We hypothesized that additional K^+ , in some form other than its borate salt, should promote complete formation of borate diesters and the G4-quartets, which should cooperatively enhance fiber formation and thereby increase the strength of the GB hydrogel.

As shown in Figure 6, the melting temperature (T_m) of the GB hydrogel made from a 2:1 mixture of G **1** and $\text{KB}(\text{OH})_4$ increased upon addition of KCl. This gel-to-sol transition temperature, as measured by standard "inverted vial-tests", increased as a function of $[\text{K}^+]$ until 2 equiv of KCl had been added to the mixture (Figure 6A). A similar increase in the hydrogel's T_m was also observed when KNO_3 was added as the K^+ source, suggesting that this phenomenon was due to the additional K^+ , which could fully saturate the borate diester and G4-quartet binding sites (Figure 6B). Importantly, addition of excess $\text{KB}(\text{OH})_4$ beyond 0.5 equiv had the opposite effect on the hydrogel's stability. Thus, the GB hydrogel made from a 2:1 mixture of G **1** and $\text{KB}(\text{OH})_4$ melted at 58.1 °C, whereas the T_m of the system containing an additional equiv of $\text{KB}(\text{OH})_4$ dropped to 40.8 °C, representing a significant decrease in gel stability.

The above observations can be rationalized by considering the structural implication of adding extra K^+ or $\text{B}(\text{OH})_4^-$ to the GB hydrogel (Figure 7). The increase in T_m values, upon addition of KCl or KNO_3 , is presumably the result of the increased stabilization of the G4-quartet and anionic borate ester units within the hydrogel. This would ultimately lead to an increase in fibril formation and thus gel strength. Conversely, addition of extra $\text{KB}(\text{OH})_4$ beyond the 2:1 G **1**:borate ratio would shift the equilibrium toward forming more

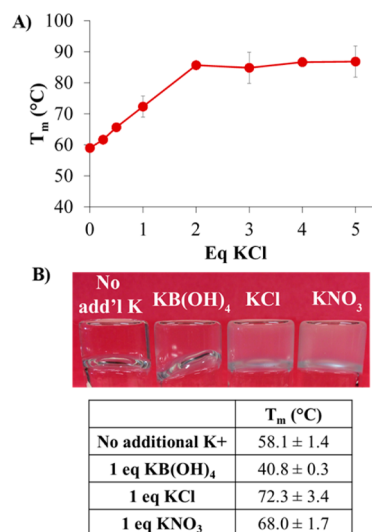


Figure 6. Addition of KCl strengthens the GB hydrogel. The melting temperature (T_m) of a 1 wt % K^+ GB hydrogel (36 mM G **1**, 18 mM $\text{KB}(\text{OH})_4$) increases as a function of KCl concentration (A). The maximum T_m is seen at 2 equiv. KCl (72 mM) at which point the T_m has increased from 58.1 to 85.6 °C (B). The GB gels with extra KCl or KNO_3 were more opaque (vial KNO_3 and KCl) than the control (vial No add'l K). Conversely, upon adding an supplemental equiv of $\text{KB}(\text{OH})_4$ (36 mM) to the gel, the T_m decreased by 17.3 °C, and the gel was visibly weaker than the control (vial $\text{KB}(\text{OH})_4$).

GB monoester **2** at the expense of the borate diesters **3/4**. Since the GB diesters **3/4** are the major borate species in the gel network, dissociation of any borate diesters **3/4** to give GB monoester **2** would weaken the GB hydrogel and lower its melting point.

To probe this rationale, we assessed the structural ramifications of adding extra K^+ or $\text{B}(\text{OH})_4^-$ to the GB gel by CD spectroscopy. As anticipated, addition of 1 equiv of either KCl or KNO_3 to the K^+ GB hydrogel resulted in an increase in the G4-quartet's characteristic CD signal near 260 nm (Figure 7). In sharp contrast the G4-quartet's CD signal at ~ 260 nm was significantly reduced relative to other peaks at 280 and the red-shifted peak at 310 nm when a supplemental equiv of $\text{KB}(\text{OH})_4$ was added. Thus, the data shown in Figure 6 are consistent with the proposal that additional K^+ helps promote and stabilize both the borate diester bonds and the G4-quartet structures, which are the key building blocks for the hydrogel's fibrous network.

Fluorescence of Thioflavin T Is Useful for Monitoring Hydrogelation Triggered by Guanosine **1.** In an earlier communication, we showed that the GB hydrogel binds cationic dyes.²⁶ In this study, we explored whether thioflavin T (ThT **6**) could be used to sense formation of G4-quartets during the self-assembly process that leads to hydrogel formation. ThT **6** is a benzothiazolium derivative that has been used as a selective indicator for G-quadruplex DNA.^{50–53} Upon binding to G-quadruplex DNA, ThT **6** displays a strong enhancement in fluorescence. Because this ThT assay is established for G-quadruplex DNA,^{49–52} we reasoned that this protocol might be useful for identifying G4-quartet assembly by guanosine itself.

Without any G **1** in solution ThT **6** was not fluorescent (Figure S3, Supporting Information). But, as shown in Figure 8, the fluorescence of ThT increased significantly in solutions that contained G **1** (0.4 wt %, 14.4 mM) and alkali borates (7.2

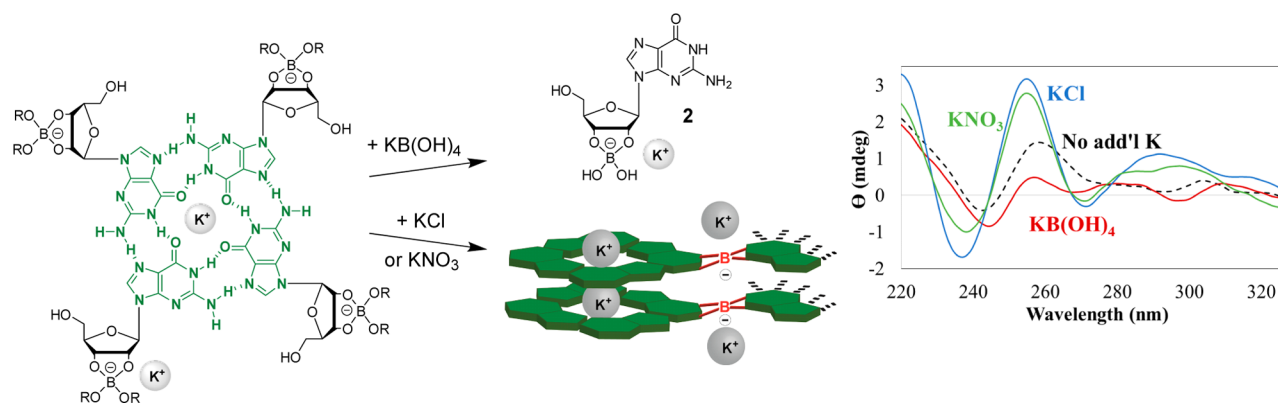


Figure 7. Addition of KCl or KNO_3 stabilizes the G4-assemblies and the anionic GB diesters **3/4** within the GB hydrogel. Conversely, KB(OH)_4 addition results in the formation of GB monoesters **2** at the expense of the GB diesters **3/4**, a key building block of the gel network, ultimately destabilizing the hydrogel. The CD spectra of these systems (36 mM **G 1**, 18 mM KB(OH)_4) provide evidence for this proposed mechanism. While the intensity of the G4-quartet CD signature increases and sharpens in the presence of KCl and KNO_3 (36 mM), these signals notably decrease with additional KB(OH)_4 (36 mM).

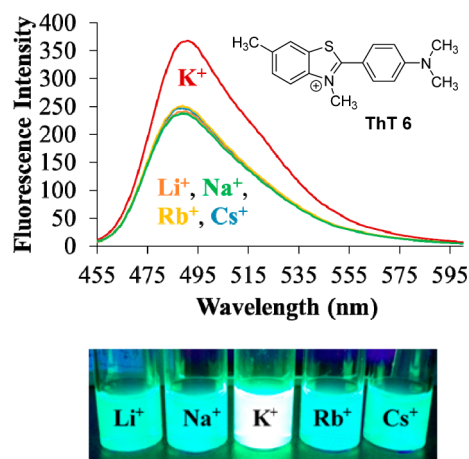


Figure 8. ThT fluorescence is cation dependent. This is apparent spectroscopically (top; 5 μM ThT **6**) and visually (bottom; 100 μM ThT **6**) at 0.4 wt % **G 1** (14.4 mM **G 1**; 7.2 mM MB(OH)_4). The highest fluorescence is seen for the K^+ GB hydrogel, suggesting it has the largest number of G4-quartets at this concentration.

mM). These solutions are at gelator concentrations of **G 1** that are below where a hydrogel is formed, indicating that the ThT is likely binding to soluble G4-quadruplex fragments that are precursors to the fully formed hydrogel network. In addition, there was an obvious difference, both spectroscopically and visually, in the fluorescence intensity of the **G 1**- KB(OH)_4 sample as compared to solutions of **G 1** that contained the other borate salts (Li^+ , Na^+ , Rb^+ , Cs^+). While ThT **6** fluoresced at 490 nm in all the solutions of **G 1**- MB(OH)_4 (14.4 mM **G 1**; 7.2 mM MB(OH)_4 ; 0.05 mM ThT **6**), the **G 1**- KB(OH)_4 showed a ~ 1.7 fold enhancement in its relative fluorescence intensity over the other metal borate complexes (Figure 8). This selectivity for K^+ was clearly apparent when various samples (14.4 mM **G 1**; 7.2 mM MB(OH)_4 ; 0.1 mM ThT **6**) were illuminated with UV light from a hand-held lamp. This enhanced fluorescence at 490 nm is consistent with the cationic ThT **6** binding to G4-quartets that are present in solutions containing **G 1** and the alkali borates. The data in Figure 8 also indicates that while all the MB(OH)_4 salts can template formation of G4-quartets by **G 1**, it is the K^+ salt that is the most efficient.

Encouraged by these observations, we employed the ThT assay to monitor hydrogelation triggered by **G 1** and KB(OH)_4 . To do so, we measured the fluorescence of ThT **6** as a function of the concentration of **G 1** (while maintaining a 2:1 **G 1**: KB(OH)_4 ratio). Figure 9 shows a concentration-dependent

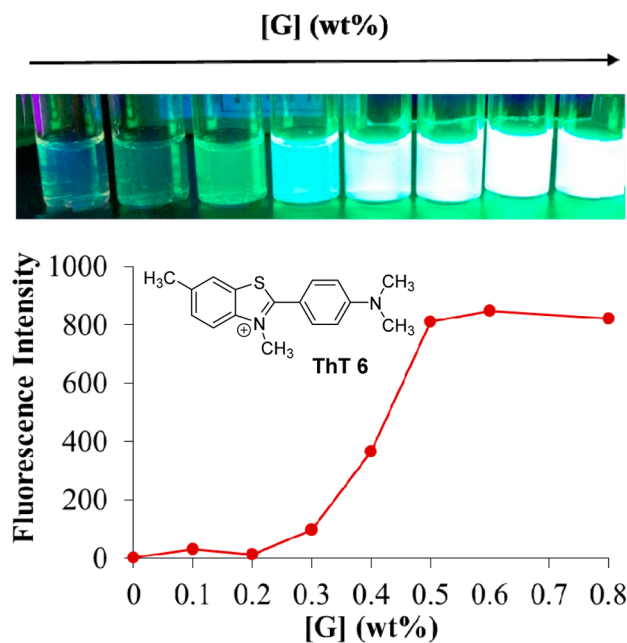


Figure 9. ThT **6** fluorescence increases with **G 1** concentration. This can be seen visually under a UV lamp as we increase the concentration of **G 1** from 0.1 to 0.8 wt % (100 μM ThT) (top). The fluorescence intensity at 490 nm begins to increase around 0.3–0.4 wt % **G 1** correlating closely with the gel point of our GB hydrogel. ThT **6** fluorescence plateaus at ~ 0.5 wt % **G 1** (bottom; 5 μM ThT).

increase in the fluorescence of ThT **6**, with the most dramatic change occurring in solutions between 0.3 and 0.5 wt % of **G 1**. In solutions with less than 0.3 wt % (10.8 mM) of **G 1**, the fluorescence of ThT **6** was near zero. However, between 0.3 and 0.4 wt %, fluorescence at 490 nm increased significantly and then leveled off at concentrations of 0.5 wt % of **G 1**. This spike in the solution's fluorescence intensity, with a midpoint near 0.4 wt % of **G 1**, corresponds with the critical gelation

concentration (CGC) of the same G 1-KB(OH)₄ system that we determined from solution viscosity measurements (Figure S4, Supporting Information). Overall, this ThT assay is convenient for monitoring the hydrogelation process involving G 1 and alkali borates. It will be interesting to see if the assay can be applied to other guanosine-based hydrogels, especially the classic 5'-GMP-K⁺ system.

CONCLUSIONS

Combining G 1 and 0.5 mol equiv of KB(OH)₄ together in water gives a true hydrogel, a transparent material with an established 3D fibrous network and a high storage modulus. The physical properties of the GB hydrogel can be modulated simply by varying the borate salt's cation. Co-addition of KB(OH)₄ gave the strongest GB hydrogel, whereas replacement with LiB(OH)₄ gave a much weaker material. The data that we presented in this paper indicate that the cation's impact on gel stability is due to its role in stabilizing both the anionic borate diesters 3/4 and the G4-quartet units that are the key building blocks for this supramolecular hydrogel. We plan to continue to explore the ability of various cations, anions and guanosine derivatives to modulate the structural and functional properties of these GB hydrogels. We also found that the G4-quartet ligand, ThT 6, fluoresces in the presence of both the GB hydrogel and its soluble G4-quadruplex precursors. The largest fluorescence response was observed in the K⁺ system, presumably due to the increased number and stability of G4-quartets and the enhanced binding opportunities for ThT 6 when this cation is present. The fluorescence intensity increased as a function of G 1 concentration, allowing us to easily measure the sol-gel transition for this system. Thus, this ThT assay can provide valuable insight into gel formation by G4-quartet based systems. In the future, we hope to further investigate the interactions of ThT 6 and other ligands with these GB hydrogels and determine if incorporating these "small molecules" into the gel network will alter the structure and properties of these supramolecular GB hydrogels.

ASSOCIATED CONTENT

Supporting Information

Experimental details and Figures S1–S4. This material is available free of charge via the Internet at <http://pubs.acs.org>.

AUTHOR INFORMATION

Corresponding Author

*jdavis@umd.edu

Notes

The authors declare no competing financial interest.

ACKNOWLEDGMENTS

This work was supported by the US DOE [DE-FG01-98ER14888] and EPSRC (EP/K003674/1). G.P. thanks the US Dept. of Education for a GAANN fellowship. We thank Wonseok Hwang and Prof. Lawrence Sita for their help with the rheology, and we thank TA Instruments (New Castle, DE) for providing the rheometer.

REFERENCES

(1) For some recent reviews on the development and characterization of supramolecular hydrogels, see: (a) Weiss, R. G. *J. Am. Chem. Soc.* **2014**, *136*, 7519–7530. (b) Raeburn, J.; Adams, D. J. *Chem. Commun.* **2014**, *51*, 5170–5180. (c) Cornwell, D. J.; Smith, D. K.

Mater. Horiz. **2015**, DOI: 10.1039/C4MH00245H. (d) Babu, S. S.; Praveen, V. K.; Ajayaghosh, A. *Chem. Rev.* **2014**, *114*, 1973–2129. (e) Estroff, L. A.; Hamilton, A. D. *Chem. Soc. Rev.* **2004**, *104*, 1201–1216. (f) Yu, G.; Yan, X.; Han, C.; Huang, F. *Chem. Soc. Rev.* **2013**, *42*, 6697–6722. (g) Buerkle, L. E.; Rowan, S. J. *Chem. Soc. Rev.* **2012**, *41*, 6089–6102. (h) Steed, J. W. *Chem. Commun.* **2011**, *47*, 1379–1383. (i) Shapiro, Y. E. *Prog. Polym. Sci.* **2011**, *36*, 1184–1253.

(2) (a) Caran, K. L.; Lee, D.-C.; Weiss, R. G. *Molecular Gels and their Fibrillar Networks*. In *Soft Fibrillar Materials: Fabrication and Applications*; Liu, X. Y., Li, J.-L., Eds.; Wiley-VCH Verlag GmbH & Co. KGaA: Weinheim, Germany, 2013. (b) *Molecular Gels: Materials with Self-Assembled Fibrillar Networks*; Weiss, R. G., Terech, P., Eds.; Springer: Dordrecht, The Netherlands, 2006. (c) Raghavan, S. R.; Douglas, J. F. *Soft Matter* **2012**, *8*, 8539–8546.

(3) (a) Ikeda, M.; Tanida, T.; Yoshii, T.; Kurotani, K.; Onogi, S.; Urayama, K.; Hamachi, I. *Nat. Chem.* **2014**, *6*, 511–518. (4) Guo, M.; Pitet, L. M.; Wyss, H. M.; Vos, M.; Dankers, P. Y. W.; Meijer, E. W. *J. Am. Chem. Soc.* **2014**, *136*, 6969–6977. (5) Guo, W.; Lu, C.-H.; Qi, X.-J.; Orbach, R.; Fadeev, M.; Yang, H.-H.; Willner, I. *Angew. Chem., Int. Ed.* **2014**, *53*, 10134–10138. (6) Yoshii, T.; Ikeda, M.; Hamachi, I. *Angew. Chem., Int. Ed.* **2014**, *53*, 7264–7267. (7) Yang, Z.; Liang, G.; Xu, B. *Acc. Chem. Res.* **2008**, *41*, 315–326. (8) Ghossoub, A.; Lehn, J.-M. *Chem. Commun.* **2005**, *46*, 5763–5765. (9) Yoshii, T.; Onogi, S.; Shigemitsu, H.; Hamachi, I. *J. Am. Chem. Soc.* **2015**, *137*, 3360–3365. (10) Liu, G.-F.; Zhang, D.; Feng, C.-L. *Angew. Chem., Int. Ed.* **2014**, *53*, 7789–7793. (11) Kuang, Y.; Shi, J.; Li, J.; Alberti, K. A.; Xu, Q.; Xu, B. *Angew. Chem., Int. Ed.* **2014**, *53*, 8104–8107. (12) Buerkle, L. E.; von Recum, H. A.; Rowan, S. J. *Chem. Sci.* **2012**, *3*, 564–572. (13) Ikeda, M.; Yoshii, T.; Matsui, T.; Tanida, T.; Komatsu, H.; Hamachi, I. *J. Am. Chem. Soc.* **2011**, *133*, 1670–1673. (14) For some recent reviews on applications of supramolecular hydrogels, see: (a) Lau, H. K.; Kiick, K. L. *Biomacromolecules* **2015**, *16*, 28–42. (b) Skilling, K. J.; Citossi, F.; Bradshaw, T. D.; Ashford, M.; Kellam, B.; Marlow, M. *Soft Matter* **2014**, *10*, 237–256. (c) Hirst, A. R.; Escuder, B.; Miravet, J. F.; Smith, D. K. *Angew. Chem., Int. Ed.* **2008**, *47*, 8002–8018. (d) Sangeetha, N. M.; Maitra, U. *Chem. Soc. Rev.* **2005**, *34*, 821–836. (15) Du, X.; Zhou, J.; Xu, B. *Chem.—Asian J.* **2014**, *9*, 1446–1472. (16) Araki, K.; Yoshikawa, I. *Top. Curr. Chem.* **2005**, *256*, 133–165. (17) (a) Bang, I. *Biochem. Z.* **1910**, *26*, 293–311. (b) Gellert, M.; Lipsitt, M. N.; Davies, D. R. *Proc. Natl. Acad. Sci. U. S. A.* **1962**, *48*, 2013–2018. (c) Davis, J. T. *Angew. Chem., Int. Ed.* **2004**, *43*, 669–698. (18) Chantot, J.-F.; Guschlbauer, W. *FEBS Lett.* **1969**, *4*, 173–176. (19) Sreenivasachary, N.; Lehn, J.-M. *Proc. Natl. Acad. Sci. U. S. A.* **2005**, *102*, 5938–5943. (20) Kawn, I. C. M.; Delley, R. J.; Hodgson, D. R. W.; Wu, G. *Chem. Commun.* **2011**, *47*, 3882–3884. (21) Yu, Y.; Nakamura, D.; DeBoyace, K.; Neisius, A. W.; McGown, L. B. *J. Phys. Chem. B* **2008**, *112*, 1130–1134. (22) Buerkle, L. E.; Li, Z.; Jamieson, A. M.; Rowan, S. J. *Langmuir* **2009**, *25*, 8833–8840. (23) Li, Z.; Buerkle, L. E.; Orseno, M. R.; Streltzyk, K. A.; Seifert, S.; Jamieson, A. M.; Rowan, S. J. *Langmuir* **2010**, *26*, 10093–10101. (24) Way, A. E.; Korpusik, A. B.; Dorsey, T. B.; Buerkle, L. E.; von Recum, H.; Rowan, S. J. *Macromolecules* **2014**, *47*, 1810–1818. (25) Okano, T.; Komatsu, T.; Nara, T.; Tsuji, K. *Yakugaku Zasshi* **1970**, *90*, 1542–1548. (26) Peters, G. M.; Skala, L. P.; Plank, T. N.; Hyman, B. J.; Reddy, G. N. M.; Marsh, A.; Brown, S. P.; Davis, J. T. *J. Am. Chem. Soc.* **2014**, *136*, 12596–12599. (27) Das, R. N.; Kumar, Y. P.; Pagoti, S.; Patil, A. J.; Dash, J. *Chem.—Eur. J.* **2012**, *18*, 6008–6014. (28) Adhikari, B.; Shah, A.; Kraatz, H.-B. *J. Mater. Chem. B* **2014**, *2*, 4802–4810.

- (29) Das, J.; Patil, A. J.; Das, R. N.; Dowdall, F. L.; Mann, S. *Soft Matter* **2011**, *7*, 8120–8126.
- (30) Dowling, V. A.; Charles, J. A. M.; Nwakpuda, E.; McGowan, L. B. *Anal. Chem.* **2004**, *76*, 4558–4563.
- (31) Case, W. S.; Glinert, K. D.; LaBarge, S.; McGowan, L. B. *Electrophoresis* **2007**, *28*, 3008–3016.
- (32) Zhang, X.; McGowan, L. B. *Electrophoresis* **2013**, *34*, 1778–1786.
- (33) Buchs, B.; Fieber, W.; Vigouroux-Elie, F.; Sreenivasachary, N.; Lehn, J.-M.; Herrmann, A. *Org. Biomol. Chem.* **2011**, *9*, 2906–2919.
- (34) Sreenivasachary, N.; Lehn, J.-M. *Chem.—Asian J.* **2008**, *3*, 134–139.
- (35) Meng, L.; Liu, K.; Mao, Y.; Yi, T. *Org. Biomol. Chem.* **2013**, *11*, 1525–1532.
- (36) Yoshikawa, I.; Yanagi, S.; Yamaji, Y.; Araki, K. *Tetrahedron* **2007**, *63*, 7474–7481.
- (37) Simeone, L.; Milano, D.; De Napoli, L.; Irace, C.; Di Pascale, A.; Boccalon, M.; Tecilla, P.; Montesarchio, D. *Chem.—Eur. J.* **2011**, *17*, 13854–13865.
- (38) Arnal-Hérault, C.; Pasc, A.; Michau, M.; Cot, D.; Petit, E.; Barboiu, M. *Angew. Chem., Int. Ed.* **2007**, *46*, 8409–8413.
- (39) The G4-quartet and relatives form assemblies with unique properties: (a) Sessler, J. L.; Lawrence, C. M.; Jayawickramarajah, J. *Chem. Soc. Rev.* **2007**, *36*, 314–325. (b) Arnal-Hérault, C.; Banu, A.; Barboiu, M.; Michau, M.; van der Lee, A. *Angew. Chem., Int. Ed.* **2007**, *46*, 4268–4272. (c) García-Arriaga, M.; Hogley, G.; Rivera, J. R. *J. Am. Chem. Soc.* **2008**, *130*, 10492–10493. (d) Ciesielski, A.; Lena, S.; Masiero, S.; Spada, G. P.; Samori, P. *Angew. Chem., Int. Ed. Engl.* **2010**, *49*, 1963–1966. (e) Cafferty, B. J.; Gallego, I.; Chen, M. C.; Farley, K. I.; Eritja, R.; Hud, N. V. *J. Am. Chem. Soc.* **2013**, *135*, 2447–2450. (f) Mihai, S.; Le Duc, Y.; Cot, D.; Barboiu, M. *J. Mater. Chem.* **2010**, *20*, 9443–9448. (g) Mihai, S.; Cazacu, A.; Arnal-Hérault, C.; Nasr, G.; Meffre, A.; van der Lee, A.; Barboiu, M. *New J. Chem.* **2009**, *33*, 2355–2343.
- (40) Schott, H. *Angew. Chem., Int. Ed. Engl.* **1972**, *11*, 824–825.
- (41) Ricardo, A.; Carrigan, M. A.; Olcott, A. N.; Benner, S. A. *Science* **2004**, *303*, 196.
- (42) Kim, H.-J.; Ricardo, A.; Illangkoon, H. I.; Kim, M. J.; Carrigan, M. A.; Frye, F.; Benner, S. A. *J. Am. Chem. Soc.* **2011**, *133*, 9457–9468.
- (43) Wada, T.; Minamimoto, N.; Inaki, Y.; Inoue, Y. *J. Am. Chem. Soc.* **2000**, *122*, 6900–6910.
- (44) Brown, S. P. *Solid State Nucl. Magn. Reson.* **2012**, *41*, 1–27.
- (45) Brown, S. P. *Prog. Nucl. Magn. Reson. Spectrosc.* **2007**, *50*, 199–251.
- (46) Webber, A. L.; Masiero, S.; Pieraccini, S.; Burley, J. C.; Tatton, A. S.; Iuga, D.; Pham, T. N.; Spada, G. P.; Brown, S. P. *J. Am. Chem. Soc.* **2011**, *133*, 19777–19795.
- (47) Peters, G. M.; Davis, J. T. *Supramol. Chem.* **2014**, *26*, 286–295.
- (48) Benner, K.; Klufers, P. *Carbohydr. Res.* **2000**, *327*, 287–292.
- (49) (a) Gabe, S. A.; London, R. E. *J. Biol. Inorg. Chem.* **2008**, *13*, 207–217. (b) Wada, T.; Sato, H.; Inoue, Y. *Biopolymers* **2004**, *76*, 15–20.
- (50) Mohanty, J.; Barooah, N.; Dhamodharan, V.; Harikrishna, S.; Pradeepkumar, P. I.; Bhasikuttan, A. C. *J. Am. Chem. Soc.* **2013**, *135*, 367–376.
- (51) de la Faverie, A. R.; Guédin, A.; Bedrat, A.; Yatsunyk, L. A.; Mergny, J.-L. *Nucleic Acids Res.* **2014**, *42*, 1–8.
- (52) Zhao, D.; Dong, X.; Jiang, N.; Zhang, D.; Liu, C. *Nucleic Acids Res.* **2014**, *42*, 11612–11621.
- (53) Bhasikuttan, A. C.; Mohanty, J. *Chem. Commun.* **2015**, DOI: 10.1039/C4CC10030A.

Supporting Information for:

G₄-Quartet•M⁺ Borate Hydrogels

Gretchen Marie Peters,[†] Luke P. Skala,[†] Taylor N. Plank,[†] Hyuntaek Oh,[‡] G. N. Manjunatha Reddy,[§]
Andrew Marsh,[#] Steven P. Brown,[§] Srinivasa R. Raghavan,[‡] and Jeffery T. Davis^{*,†}

[†]Department of Chemistry & Biochemistry and [‡]Department of Chemical & Biomolecular Engineering, University of Maryland, College Park, MD 20742 USA

[§]Department of Physics and [#]Department of Chemistry, University of Warwick, Coventry CV4 7AL, UK
*jdavis@umd.edu

Table of Contents

General Experimental	S2
General Procedure for Gel Preparation	S2
Procedure for Solid-State NMR experiments	S3
Procedure for Small-Angle Neutron Scattering (SANS) Measurements	S3
Rheology Procedure	S4
Procedure for Variable Temperature ¹ H and ¹¹ B NMR Melting Experiment	S4
Procedure for Diffusion-Ordered Spectroscopy Measurements	S5
Procedure for Powder X-Ray Diffraction	S5
Figure S1. Powder X-Ray Diffraction Spectrum of 0.4 wt% G 1 •KB(OH) ₄	S6
Procedure for Melting Point Determination	S7
Procedure for Circular Dichroism Spectroscopy Measurements	S7
Figure S2. SANS profiles for 2 wt% G 1 •KB(OH) ₄ and G 1 •TAcG 5 binary gel	S8
Procedure for Thioflavin T 6 assays	S9
Viscometry Procedure	S9
Figure S3. Thioflavin T 6 with and without GB hydrogel	S10
Figure S4. Apparent viscosity as a function of G 1 •KB(OH) ₄ concentration	S11
Supporting Information References	S11

General experimental: All ^1H solution-state NMR spectra were recorded on a Bruker DRX-400 operating at 400.13 MHz or a Bruker AVIII-600 operating at 600.13 MHz. Chemical shifts are reported in ppm relative to the residual solvent peak. For ^{11}B solution-state NMR spectra, chemical shifts are reported in ppm relative to $\text{BF}_3 \cdot \text{O}(\text{C}_2\text{H}_5)_2$. Deuterated solvents were purchased from Cambridge Isotope Labs. Circular dichroism spectroscopy was performed on a Jasco J-810 spectropolarimeter. Fluorescence spectroscopy measurements were made on a Hitachi F-4500 fluorescence spectrophotometer. All rheological data was collected using an AR2000 stress-controlled rheometer from TA instruments. Chemicals and solvents were purchased from Santa Cruz Biotechnology, Aldrich, Fisher, and Acros.

General Procedure for Gel Preparation: Guanosine **1** was weighed into a vial, and the appropriate amount of $\text{B}(\text{OH})_3$ solution (and water if necessary) was added. The mixture was sonicated for approximately 30 s, and the appropriate amount of MOH (M=Li, Na, K, Rb, Cs) solution was added. The suspension was heated to 90 - 100 °C in a water bath until all material was dissolved, and the solution was clear. The solution was then removed from the heat bath and allowed to cool to room temperature. Unless otherwise noted, gels were formed using a 2:1 ratio of G **1**: $\text{MB}(\text{OH})_4$.

Procedure for Solid-State NMR Experiments: Solid-state NMR experiments were performed on a Bruker Avance II+ spectrometer operating at a ^1H Larmor frequency of 600 MHz using a 1.3 mm MAS probe operating in double-resonance mode. A Gel sample (2 wt% G·KB(OH)₄ in H₂O) was prepared according to the gel preparation procedure. The gel was then formed into a cube and soaked in 155 mM KCl for 24 h. Following the soak, the gel was lyophilized to a white powder. Approximately 2 mg of lyophilized powder were packed into a 1.3 mm (o.d) Zirconia rotor. For ^1H Double-Quantum (DQ) Magic-Angle Spinning (MAS) experiments,^[1] the excitation and reconversion of DQ coherence was achieved using one rotor period of BABA (back-to-back) recoupling.^[2,3] A ^1H nutation frequency of 100 kHz was used corresponding to a ^1H 90° pulse duration of 2.5 μs . A 16-step phase cycle was used to select $\Delta p = \pm 2$ on the DQ excitation pulses (4 steps) and $\Delta p = \pm 1$ (4 steps) on the z -filter 90° pulse, where p is the coherence order. For each of 256 t_1 FIDs, 16 transients were co-added. A rotor-synchronized t_1 increment of 16.7 μs was used, with the States method being employed to achieve sign discrimination in the DQ dimension. A recycle delay of 2 s was used, corresponding to an experimental time of 2 h.

Procedure for Small-Angle Neutron Scattering Measurements: GB gels and TAcG 5: G 1 binary mixtures were prepared at 2 wt% according to the general gel preparation or literature procedures, respectively.^[4] SANS measurements were made on the NG-7 (30 m) beamline at National Institute of Standards and Technology (NIST) in Gaithersburg, MD. Neutrons with a wavelength of 6 Å were selected. Three sample-detector distances (1 m, 4 m, and 15 m) were used to probe a wide range of wave vectors from 0.004 to 0.4 Å⁻¹. Samples were studied in 2 mm quartz cells at 25 °C. The scattering spectra were corrected and placed on an absolute scale using calibration standards provided by NIST. The data are shown for the radially averaged intensity I as a function of the wave vector $q = (4\pi/\lambda)\sin(\theta/2)$, where l is the neutron wavelength and θ is the scattering angle.

Rheology Procedure: Gels were prepared at 2 wt% (72 mM G **1**; 36 mM MB(OH)₄, M = K or Li) following the general gel procedure. Rheological experiments were performed at 20 °C using parallel plate geometry (20 mm diameter) and a solvent trap to minimize sample drying during measurements. The gel samples were allowed to equilibrate on the plate for 10 min. Frequency sweeps were performed at 1% strain. Stress sweeps were performed at 10 rad/sec by ramping the stress from 0.5 to 1000 Pa.

Procedure for Variable Temperature ¹H and ¹¹B NMR Melting Experiments: GB hydrogels (50 mM G **1**; 25 mM MB(OH)₄) were prepared in D₂O according to the general gel preparation procedure. The warm gel (0.5 mL) was then transferred into an NMR tube, a DMSO internal standard contained within a melting point capillary tube was added, and the gel was allowed to cool overnight. ¹H NMR spectra (25 co-added transients, 25 s delay) were obtained from 15 to 85 °C or until the amount of G **1** in solution remained constant. Samples were spun while heating to help prevent bubble formation. The concentration of the target in the sol phase was determined relative to the internal standard. The percent “G **1** in sol” was calculated according to the following equation:

$$\% G \mathbf{1} \text{ in sol} = \frac{[G \mathbf{1} \text{ in sol at desired } T]}{[G \mathbf{1} \text{ in sol at } 85 \text{ } ^\circ\text{C}]} * 100$$

Total concentration of each target (85 °C) was confirmed by adding 2 μL of DCl to the NMR tube and dissolving the gel. ¹¹B NMR spectra were obtained on the same samples using 1000 scans with a 90° pulse length, a relaxation delay of 0.2 s, and pre-scan delay of 8 μs. Experiments were repeated at least three times.

Procedure for Diffusion-Ordered Spectroscopy Measurements: A Na⁺ GB hydrogel (50 mM G **1**; 25mM NaB(OH)₄) was prepared in D₂O according to the general gel preparation procedure. The warm gel (0.2 mL) was then transferred into a Shigemi tube (Shigemi, Inc., Allison Park, PA), and the gel was allowed to cool overnight. Diffusion experiments were performed on a Bruker AVIII-600, using a Stimulated Echo Pulse Gradient sequence in FT mode. Experiments consisted of 32 points at 100 scans with a delay of 5 s, a gradient pulse length of 1.65 ms, and Δ value of 60.0 ms. The temperature was controlled at 45.0 °C, and the measurements were repeated at least 3 times. Diffusion coefficients were calculated by integrating of the peaks of interest and deriving a single exponential decay using the “Simfit (Bruker XWINNMR)” software.

Procedure for Powder X-Ray Diffraction: A 0.4 wt% K⁺ GB hydrogel (14.4 mM G **1**, 7.2 mM KB(OH)₄) was prepared according to the general gel procedure and lyophilized to form a white powder. X-ray powder diffraction measurements were performed with a Cu radiation source at 20 °C using a Bruker D8 Advance Bragg-Brentano Diffractometer equipped with a LynxEye detector.

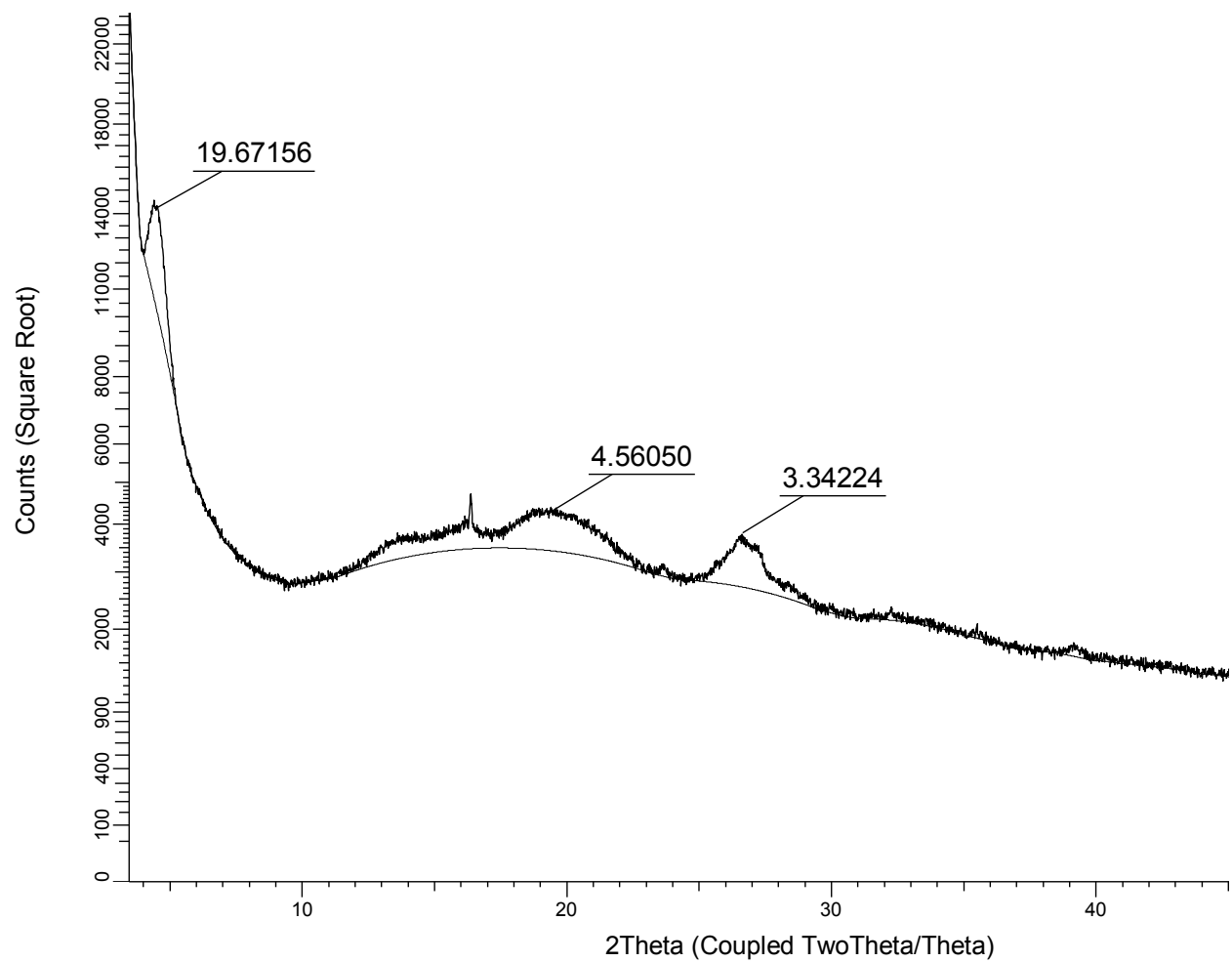


Figure S1. Powder X-ray diffraction spectrum of a lyophilized 0.4 wt% K^+ GB hydrogel (14.4 mM G **1**, 7.2 mM $KB(OH)_4$) shows evidence for G4-quartet formation. The spectrum shows a signal at $2\theta \approx 5.7^\circ$ with a corresponding distance of 19.7 Å, in line with the width of a single G4-quartet. Additionally, there is a signal at $2\theta \approx 26.8^\circ$ ($d = 3.3$ Å), which corresponds to the π - π stacking distance between two G4-quartets.

Procedure for Melting Temperature Determination: GB hydrogels (36 mM G **1**, 18 mM KB(OH)_4) were prepared in 3 mL vials according to the general gel procedure, and supplemental equivalents of KCl, KNO_3 , or KB(OH)_4 were added as necessary. Samples were allowed to cool and set for at least 24 h. The final volume of each sample was 1 mL. Wire was attached to the top of the vials with electrical tape, and the samples were suspended in a water bath. The temperature of the water bath was increased at a rate of 5 °C/min and allowed to equilibrate for 3 min before inversion. At each temperature, the vial was physically inverted to assess melting. The sample was considered “melted” when the gel flowed upon inversion and could no longer maintain the solid-like rheology. If the sample had not melted by 100 °C, the protocol was performed in an oil bath. Each measurement was repeated a minimum of 3 times.

Procedure for Circular Dichroism Spectroscopy Measurements: CD spectroscopy was performed at room temperature with a 1 wt% GB hydrogel (36 mM G **1**) prepared using general gel procedures, and supplemental equivalents of KCl, KNO_3 , or KB(OH)_4 were added as necessary. Samples were allowed to cool and set for at least 24 h. Measurements were made in a quartz Hellma 106-QS cell with 0.01 mm optical path length. Spectra were obtained using a scanning speed of 100 nm/min, response time of 2 s, and bandwidth of 1 nm. At least three scans were accumulated from 500 to 200 nm for each trial.

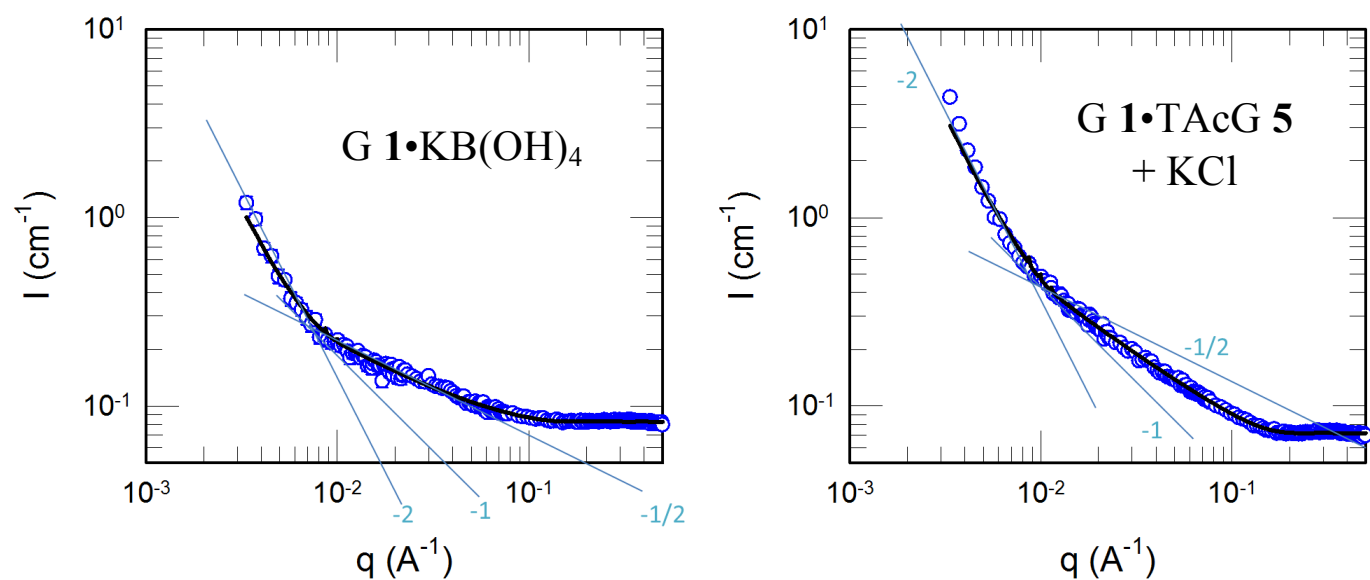


Figure S2. Small angle neutron scattering profiles of a 2 wt% G 1•KB(OH)₄ hydrogel and a 2 wt% G 1•TAcG 5 (50:50) binary gel^[4] formed with KCl. These data were fit to the flexible coil model resulting in radii of 21.5 Å and 16.9 Å, respectively. Additionally, the Kuhn length was determined to be 460 Å for the GB hydrogel and 355 Å for the G 1•TAcG 5 binary hydrogel.

Procedure for Thioflavin T 6 Assays: GB solutions were prepared at 0.8 wt% G 1 (28.8 mM G 1; 14.4 mM MB(OH)₄) according to the general procedure. While warm, the solution was transferred to a vial containing ThT 6 and diluted with water to 0.4 wt% G 1 and 5 μM ThT 6. The samples were shaken to ensure the dye distributed throughout the solution and were transferred to a quartz cuvette (10 mm path length) and allowed to cool for 2h. Emission response was recorded from 455 to 600 nm after exciting at 450 nm. Spectra were acquired at a scanning speed of 240 nm/min, a response time of 0.5 s, with slit widths of 2.5 nm. Samples for concentration dependence experiments were prepared in a similar manner, and emission was measured at 490 nm. All photographic images were obtained using 100 μM ThT.

Viscometry Procedure: All viscometry experiments were performed using Cannon Ubbelohde Semi-Micro Size 50 Viscometers. Gel solutions between 0.05-0.4 wt% in G 1 were prepared following the general gel procedure. The solutions were pipetted into the viscometer and allowed to equilibrate in the viscometer for 15 minutes. Each efflux time measurement was repeated 5 times. The average of these efflux times was multiplied by the viscometer constant provided to obtain the kinematic viscosity (η).

100 μM ThT 6 + GB- K^+

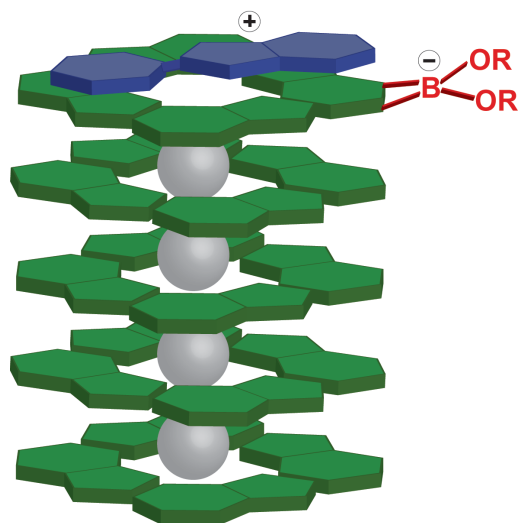


Figure S3. Thioflavin T 6 fluoresces in the presence of the GB hydrogel. While ThT 6 (100 μM) is not visibly fluorescent under a UV lamp (left, vial 100 μM ThT), when exposed to a 1 wt% K^+ GB hydrogel (36 mM G 1, 18 mM $\text{KB}(\text{OH})_4$) there is a notable fluorescence response (left, vial + GB- K^+). This is presumably due to the ability of ThT 6 to dock onto the G_4 -quartets within the GB hydrogel (right).

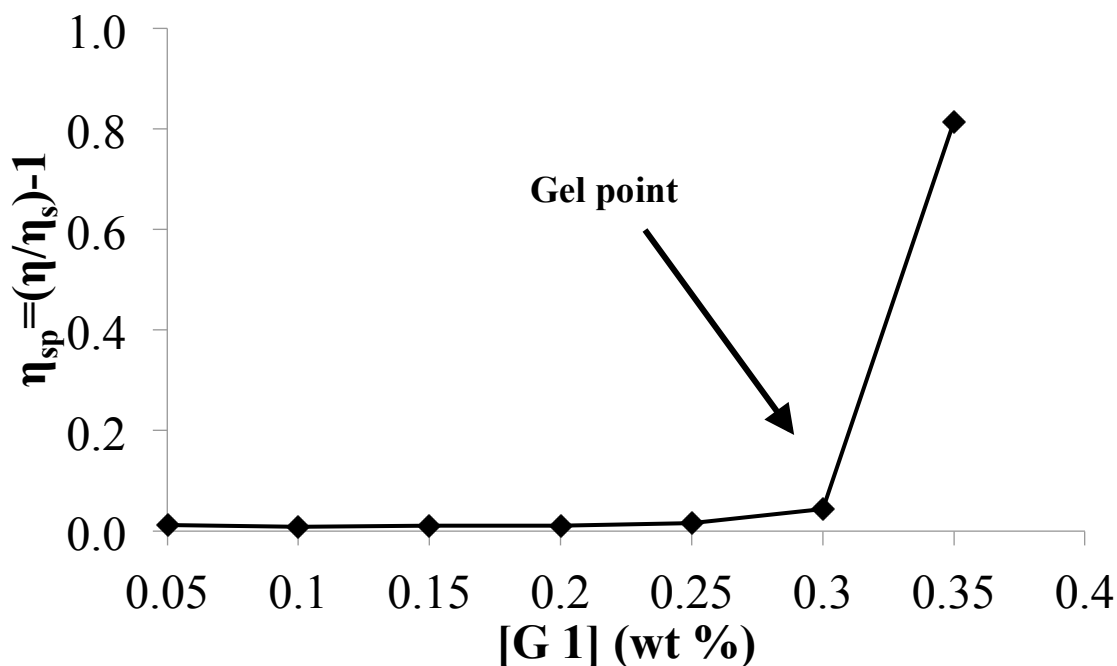


Figure S4. The apparent viscosity of the K^+ GB system dramatically increases between 0.3 and 0.35 wt% G **1** (10.8 – 12.6 mM). The viscosity was determined using the viscometry procedure described above. At concentrations below 0.3 wt% G **1**, the viscosity is indistinguishable from water and thus, η_{sp} is \sim zero. Between 0.3 – 0.35 wt% G **1**, however, η_{sp} spikes dramatically, suggesting the viscosity has increased as a result of the initiation of the fibrous network.

References:

- [1] Brown, S. P. *Prog. Nucl. Magn. Reson. Spectrosc.* **2007**, *50*, 199-251.
- [2] Sommer, W.; Gottwald, J.; Demco, D. E.; Spiess, H. W. *J. Magn. Reson. Ser. A* **1995**, *113*, 131-134.
- [3] Schnell, I.; Lupulescu, A.; Hafner, S.; Demco, D. E.; Spiess, H. W.; *J. Magn. Reson.* **1998**, *133*, 61-69.
- [4] (a) Buerkle, L. E.; Li, Z.; Jamieson, A. M.; Rowan, S. J. *Langmuir* **2009**, *25*, 8833–8840. (b) Li, Z.; Buerkle, L. E.; Orseno, M. R.; Streletzky, K. A.; Seifert, S.; Jamieson, A. M.; Rowan, S. J. *Langmuir* **2010**, *26*, 10093–10101.